Solar Physics
DOI: 10.1007/•••••-•••-•••-••••-•

Microwave Neutral Line Associated Source and a Current Sheet

A.M. Uralov[1] · **V.V. Grechnev**[1] · **G.V. Rudenko**[1] · **I.G. Rudenko**[1] · **H. Nakajima**[2]

Received ; accepted

Abstract Neutral Line associated Sources (NLS) are quasi-stationary microwave sources projected onto vicinities of the neutral line of the photospheric magnetic field. NLS are often precursors of powerful flares, but their nature is unclear. We endeavor to reveal the structure of an NLS and to analyze a physical connection between such a source with a site of energy release in the corona above NOAA 10488 (October/November 2003). Evolution of this AR includes emergence and collision of two bipolar magnetic structures, rise of the main magnetic separator, and the appearance of an NLS underneath. The NLS appears at a contact site of colliding sunspots, whose relative motion goes on, resulting in large shear along a tangent. Then the nascent NLS becomes the main source of microwave fluctuations in the AR. The NLS emission at 17 GHz is dominated by either footpoints, or the top of a loop-like structure, an NLS loop, which connects two colliding sunspots. During a considerable amount of time, the emission dominates over that footpoint of the NLS loop, where the magnetic field is stronger. At that time, the NLS resembles a usual sunspot-associated radio source, whose brightness center is displaced towards the periphery of a sunspot. Microwave emission of an X2.7 flare is mainly concentrated in an ascending flare loop, initially coinciding with the NLS loop. The top of this loop is located at the base of a non-uniform bar-like structure visible in soft X-rays and at 34 GHz at the flare onset. We reveal (*i*) upward lengthening of this bar before the flare onset, (*ii*) the motion of the top of an apparently ascending flare loop along the axis of this bar, and (*iii*) a non-thermal microwave source, whose descent along the bar was associated with the launching of a coronal ejection. We connect the bar with a probable position of a nearly vertical diffusion region, a site of maximal energy release inside an extended pre-flare current sheet. The top of the NLS loop is located at the bottom of this region. A combination of the NLS

[1] Institute of Solar-Terrestrial Physics SB RAS, Lermontov St. 126, Irkutsk 664033, Russia email: uralov@iszf.irk.ru email: grechnev@iszf.irk.ru email: rud@iszf.irk.ru email: igr@iszf.irk.ru
[2] Nobeyama Radio Observatory, Minamimaki, Minamisaku, Nagano 384-1305, Japan email: nakajima@nro.nao.ac.jp

loop and diffusion region constitutes the skeleton of a quasi-stationary microwave NLS.

Keywords: Active Regions, Magnetic Fields; Corona, Radio Emission; Electric Currents and Current Sheets; Flares, Dynamics; Flares, Pre-Flare Phenomena; Magnetic fields, Corona; Radio Bursts, Microwave (mm, cm)

1. Introduction

Neutral Line associated Sources (NLS) discovered by Kundu *et al.* (1977) are quasi-stationary, bright, rather compact microwave sources projected onto the vicinity of a neutral line of the photospheric magnetic field. NLS are one of puzzles of active regions, their nature is unclear. Properties of NLS have been studied in observations with the Westerbork Synthesis Radio Telescope at 5 GHz, the Very Large Array at 4.9, 8.4, and 15 GHz, the Siberian Solar Radio Telescope (SSRT; Smolkov *et al.*, 1986; Grechnev *et al.*, 2003) at 5.7 GHz, and with the RATAN-600 at several frequencies. Association of NLS with filaments in active regions and their possible relation to soft X-ray emitting loops, arch filament systems, emerging flux regions, and solar flares as well as their possible emission mechanisms have been discussed by Kundu and Velusamy (1980); Kundu, Schmahl, and Rao (1981); Kundu and Alissandrakis (1984); Strong, Alissandrakis, and Kundu (1984); Gelfreikh (1985); Akhmedov *et al.* (1986); Chiuderi Drago, Alissandrakis, and Hagyard (1987); Korzhavin and Vatrushin (1989); Borovik, Vatrushin, and Korzhavin (1989); Sych, Uralov, and Korzhavin (1993); Uralov *et al.* (1996a, 1998); Lee *et al.* (1997). Observations with the RATAN-600 led to a conclusion about a "peculiar" radio spectrum of such sources (Gelfreikh, 1985; Korzhavin and Vatrushin, 1989; Borovik, Vatrushin, and Korzhavin, 1989; Alissandrakis *et al.*, 1993). The peculiarity consisted in the fact that these sources could not be interpreted as the usual components of radio emission associated with sunspots, plages, or "coronal condensations" because of the very steep slope of their flux spectra toward higher frequencies. These sources had low or moderate degrees of the circular polarization (5 – 30%). The authors assumed a possible connection of peculiar radio sources with sites of energy release in magnetospheres of active regions, *e.g.*, with current sheets.

Observations of "peculiar" sources were limited to a frequency of 15 GHz that did not allow inference of the behavior, statistics, and even the existence of such or similar sources at higher frequencies. The Nobeyama Radioheliograph (NoRH; Nakajima *et al.*, 1994) operates at two higher frequencies of 17 and 34 GHz. Compact, very bright (up to 1 MK) NLS have been found at 17 GHz in ARs producing powerful long-duration flares and coronal mass ejections (Uralov *et al.*, 2000; Uralov, Rudenko, and Rudenko, 2006a, 2006b; Rudenko, Rudenko, and Uralov, 2007; Uralov *et al.*, 2007). Relations of 17 GHz NLS to sources with a "peculiar" spectrum are still unclear. Nevertheless, our experience allows us to make some remarks.

Comparisons of NoRH 17 GHz and SSRT 5.7 GHz images of ARs containing NLS revealed the following facts: masking of 5.7 GHz NLS emission by the background gyroresonance emission of ARs; displacement of NLS visible

at 17 GHz and 5.7 GHz; significant decrease of the visible size of an NLS with wavelength; sometimes only minor difference of their brightness temperatures at these frequencies (*e.g.*, 1 MK at 17 GHz and 2 – 3 MK at 5.7 GHz).

An NLS at 17 GHz can be polarized up to 90% and often resembles a normal gyroresonance source above a sunspot in intensity (Stokes I) and polarization (Stokes V) images. On the one hand, such resemblance does not contradict an assumption of appreciable contribution of gyroresonance radiation in the NLS emission in many cases. On the other hand, this complicates identification of an NLS at 17 GHz. Also, a direct comparison of microwave images with routinely observed photospheric line-of-sight magnetograms (*e.g.*, those of SOHO/MDI, Scherrer *et al.*, 1995) is not always successful. This could be due to instrumental effects. Moreover, a principal difficulty exists, because a projection effect inherent for line-of-sight magnetograms causes a displacement of a neutral line in an active region. To overcome this difficulty in studying evolution of an NLS in an active region during its passage across the solar disk, Uralov, Rudenko, and Rudenko (2006a) proposed a method to identify NLS at 17 GHz. The method employs the fact that NLS are located in regions, where the horizontal magnetic component is maximal, or close to these regions. A strong magnetic field is necessary for possible gyromagnetic emissions of an NLS at 17 GHz.

Even if emission mechanisms of an NLS were known, one could not answer what an NLS is; whether a physical connection exists between NLS and big flares and, if any, then what its nature is; what determines resemblance and differences between an NLS and a radio source associated with a quiet sunspot.

Our paper demonstrates a connection between conditions of the development of an active region, the appearance of an NLS at 17 GHz, and onsets of flares. The basic experimental material is constituted by NoRH images observed at 17 and 34 GHz. We also use SOHO/MDI magnetograms and images from the Soft X-ray Imager (SXI, Hill *et al.*, 2005) on GOES-12, and SSRT. We study the active region 10488 observed in October – November 2003. During this period, ARs 10484, 10486, and 10488 produced a series of GOES X class flares. NLS have been identified at 17 GHz in each of these active regions (total of seven such sources: Uralov, Rudenko, and Rudenko, 2006a). We study evolution of one of them.

For qualitative comparisons of microwave and magnetic structures of the AR, we employ the method of magnetic sources. This method appears to be adequate to locate an NLS and a possible current sheet within an AR, and to compare their sizes. We use an algorithm of Longcope and Silva (1998). To calculate magnetic sources, we employ the potential approach. There is, however, a general limitation of the method of magnetic sources: the radial (normal to the solar surface) component of the magnetic field should be known. For an AR located far from the solar disk center, this magnetic component must be calculated. Two methods are used in calculations of the radial component from line-of-sight magnetograms, *i.e.*, the method of Sakurai (1982) and the method of Rudenko (2001). We use the latter method. A brief description can be found in Uralov, Rudenko, and Rudenko (2006a).

We also use the potential approach to calculate magnetograms of the radial (B_r) and the magnitude of the tangential (horizontal) magnetic field (B_t) at low

coronal heights (*i.e.*, 2 Mm). Such magnetograms are useful for identification of an NLS at 17 GHz, and their use appears to be justified even for strongly sheared nonlinear force-free (NLFF) magnetic fields. Analytical models of such fields were obtained by Low and Lou (1990) and were used by Schrijver *et al.* (2006) in testing algorithms for the computation of NLFF fields in the corona. We compared B_r and B_t magnetograms calculated using the potential approach with an exact solution obtained with one of NLFF field models (Case I of the latter paper) and found satisfactory agreement within a range of heights and positions of the AR that are important for our task. In the present paper, the results obtained within the potential approach are used in qualitative judgments about the AR rather than for rigorous quantitative evaluations.

Section 2 discusses the evolution of AR 10488, pointing out its ability to produce powerful flares. In Section 3, we reveal the appearance of a 17 GHz NLS at a collision site of opposite-polarity sunspots, where the horizontal magnetic component is maximal. The NLS emission is dominated by either footpoints, or the top of an NLS loop, which connects colliding sunspots. Section 4 addresses an X2.7 flare starting with brightening footpoint of the NLS loop and subsequent appearance of a source at its top. Section 5 summarizes the results.

2. Evolution of AR 10488

Two bipolar structures successively appeared in the eastern solar hemisphere on 26 and 27 October. They approached each other, collided, and combined to form AR 10488. The AR crossed the central meridian on 28 October and reached the west limb on 4 November. An NLS appeared on 31 October at the place, where opposite-polarity sunspots, initially belonging to different bipolar structures, came into the closest contact. On 3 November, two homologous flares, an X2.7 (soft X-ray peak at 01:30) and an X3.9 (09:55; all times are UT) one occurred in this AR. Microwave images of the X2.7 flare show a flare loop growing from the NLS. The X3.9 flare occurred during the night for the NoRH.

2.1. Collision of two Magnetic Structures

MDI magnetograms presented in Figure 1 show emergence and collision of two magnetic structures that formed AR 10488. The western magnetic structure appears on 26 October (frame a). Frames b and c show emergence of the second, eastern bipolar structure (circled). The positive polarity leads in both structures. The leading-polarity region of the eastern structure, P2, approaches the immovable negative-polarity region N1 of the western structure and rounds it like an obstacle from the North. From 30 October onwards, the sunspots corresponding to P2 and N1 are comparable in size and share a penumbra. On 31 October – 1 November, at the place of their contact, an NLS appears at 17 GHz. Its approximate position is shown in Figure 1g,h.

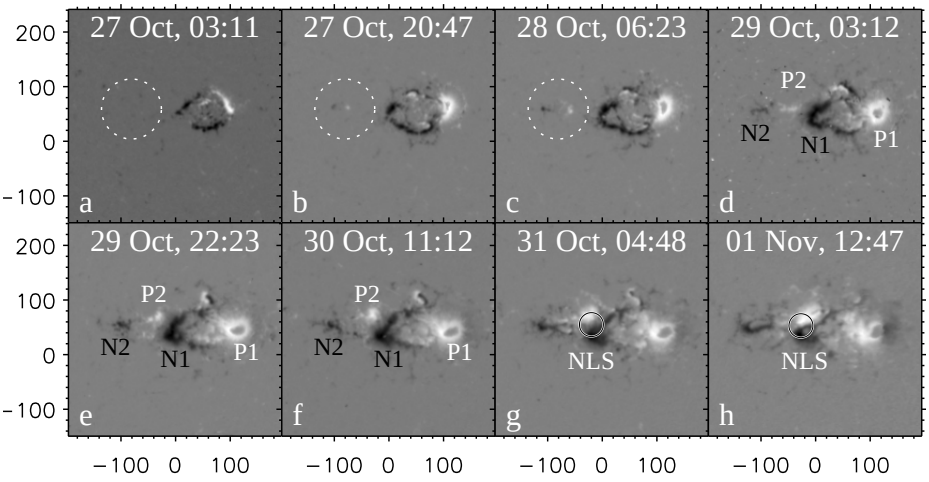

Figure 1. History of AR 10488: emergence and collision of two bipolar structures. MDI magnetograms, 27 October – 1 November (bright N, dark S). All frames are re-projected to the central meridian through compensation of the solar rotation to 28 October, 21:00. The dashed circle in frames a – c outlines the eastern dipole. The circle in frames g,h denotes the birthplace of an NLS. Axes show arcseconds from the center.

2.2. Quadrupole. Convergence, Shift, and Growth of Magnetic Sources

Figure 2 shows photospheric B_r magnetograms extrapolated from line-of-sight MDI magnetograms averaged over four pixels and re-projected to the central meridian, as done in Figure 1. AR 10488 was close to the limb on 2 November, and, especially, on 3 November that certainly worsens the quality of the extrapolated magnetograms. Contours correspond to $B_r = 100$ G and bound areas, whose magnetic fluxes dominate. These areas constitute the basis for calculations of sizes and positions of the main positive magnetic sources P1 and P2 as well as negative ones, N1 and N2. Index 1 corresponds to the magnetic sources of the western bipolar structure, and index 2 corresponds to the eastern one. Four sources form a changing quadrupole. Despite some arbitrariness of the choice of the number and positions of the sources, the domination of four main magnetic sources in the evolution of the AR clearly shows up from Figure 1. Arrangement of sources P1, N1 and N2 does not appreciable change during 29 October – 3 November. By contrast, source P2 moves significantly. The magnetic flux of source N1 is practically invariable during 29 – 31 October, and then it slightly decreases. At the same time, the magnetic flux of P2 continuously increases. One should realize that measurements of magnetic fluxes are not rigorous due to several reasons. They are, in particular, imperfectness of the potential-field approach used for extrapolation of the magnetic field and the closeness of the AR to the solar limb on 1 – 3 November. Also, MDI magnetograms cannot correctly represent strong magnetic fields typical of sunspot umbrae that show up as gray patches inside areas of P1 from 27 October on and N1 from 29 October on. Keeping in mind these circumstances, one can assert the approximate constancy of the magnetic fluxes of P1 and N1 and continuous increase of the fluxes of P2

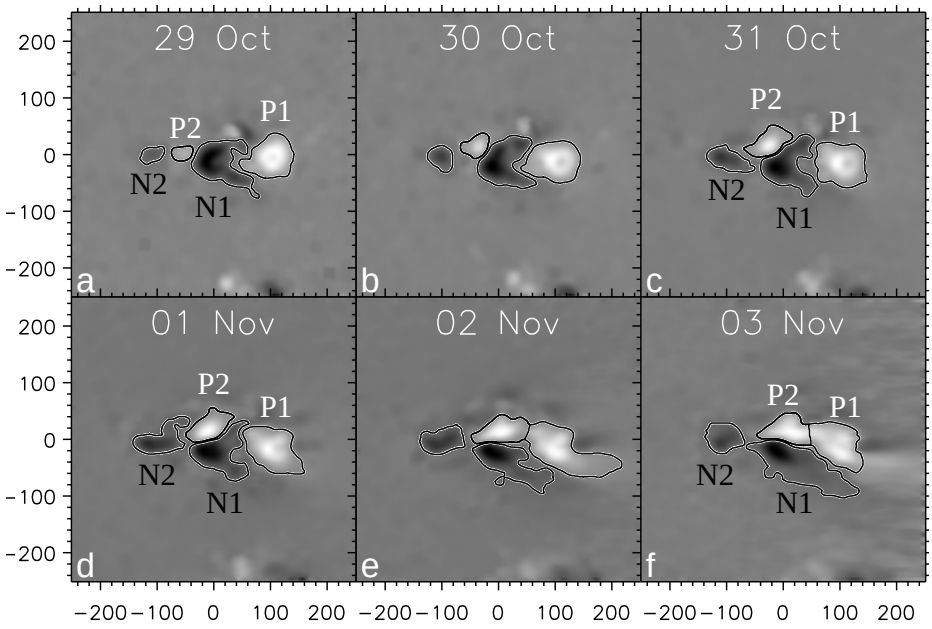

Figure 2. B_r magnetograms of AR 10488 from 29 October through 3 November (all at 04:48 UT) calculated within the potential-field approach (white N, black S). All frames are re-projected to the central meridian. Contours bound areas whose magnetic fluxes dominate. These areas constitute a basis for calculation of magnetic sources P1, P2 (positive) and N1, N2 (negative), which form a changing quadrupole. Axes show arcseconds from the center.

and N2 from 29 October to 3 November. The NLS appeared at 17 GHz on 31 October – 1 November at a contact site of magnetic areas P2 and N1. By this time, the magnetic flux of P2 becomes comparable with the flux of N1.

Figure 3 shows a separator (thick line) calculated from the B_r magnetograms of Figure 2. Footpoints of the separator at the photosphere are negative (A12) and positive (B12) null points. Thin lines show intersections of separatrix surfaces with the photosphere; in particular, spine field lines are solid. The shortness and asymmetric positions of the separator of 29 and 30 October are due to a large difference of the magnetic sources: the ratio of (P2,N2)/(P1,N1) is about 16 on 29 October and about 6 on 30 October. This difference declines, and on 1 – 3 November, the projection of the separator onto the photosphere lies almost entirely within the photospheric bottom of the central magnetic domain. A clockwise rotation of the separator is mainly caused by the motion of the magnetic source P2. From 29 October to 3 November, the height of the separator increases from ≈ 13 Mm to ≈ 70 Mm. We also calculated the topological structure of AR 10488 with 12 magnetic sources; this nearly not changed the position and shape of the main separator.

2.3. Summary of Section 2

Basically, the magnetic field of AR 10488 has a quadrupolar topology. There are two factors of changes, the growth of magnetic sources and their motion. The rise

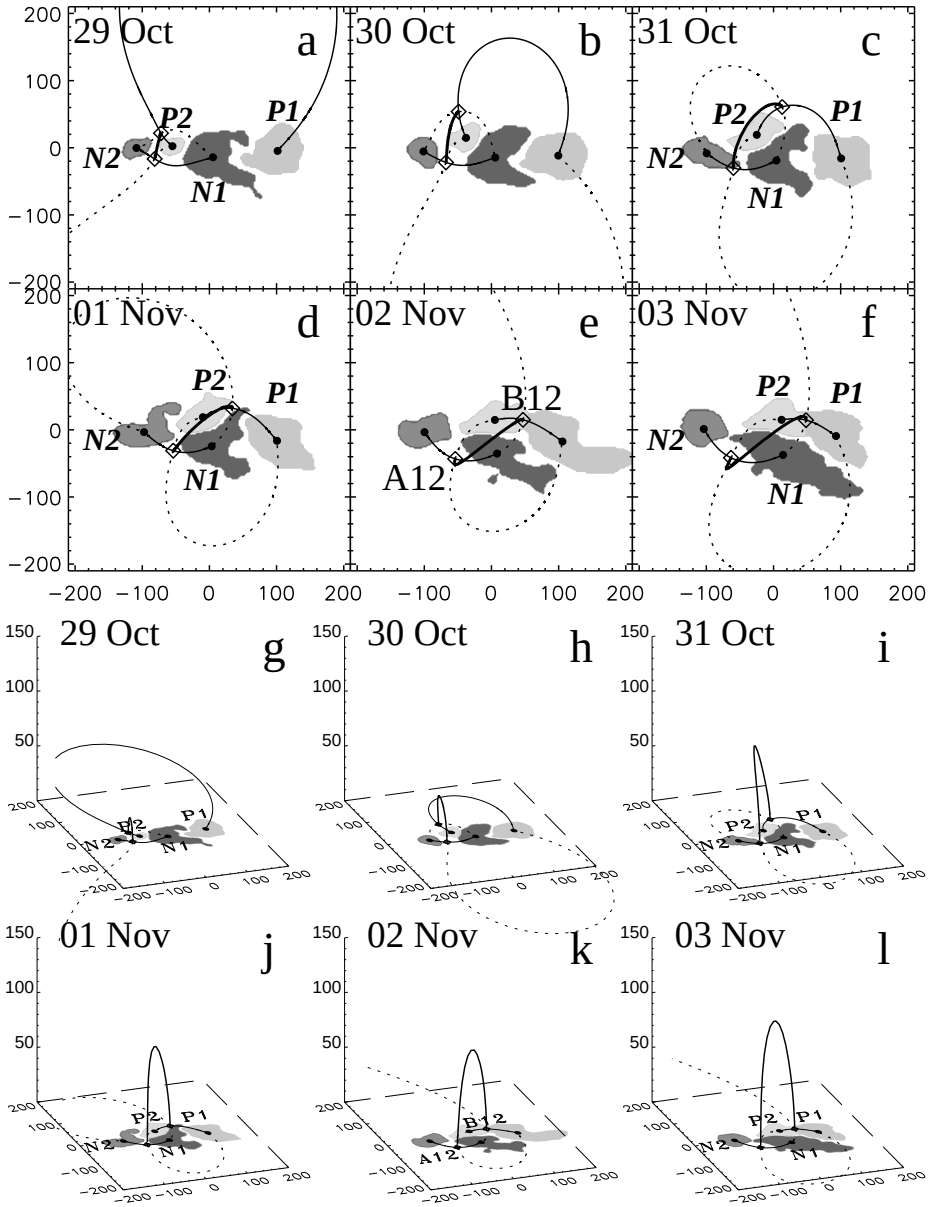

Figure 3. Magnetic field of AR 10488: top view (a – f) and side view (g – l). Thick solid line represents a magnetic separator calculated from B_r magnetograms (Figure 2). Thin solid and dotted lines show intersections of separatrix surfaces with the photosphere. A12 and B12 are null points. P1, P2, and N1, N2 are magnetic sources. Axes show arcseconds. The scale along the z-axis is enlarged.

of the magnetic separator is mainly due to growth of sources P2 and N2. This asymmetry suggests redistribution of magnetic fluxes between four magnetic domains constituting the quadrupolar magnetosphere (simultaneous change of four immovable sources by the same factor does not change the separator). Since magnetic fluxes are frozen in the plasma, redistribution is only possible via magnetic reconnection in current sheets. Thus, the rise of a separator, along with the asymmetric growth of immovable magnetic sources, inevitably implies magnetic reconnection. The motion of magnetic sources (in particular, their convergence) is well studied and is known to also cause formation of current sheets. Both these factors are clearly present in our case. Along with the presence of sufficiently strong magnetic fields, they show the ability of the AR to produce powerful flares.

3. Neutral Line associated Source

We firstly make a remark about the term of "Neutral Line associated Source". It hints at the position of a 17 GHz NLS right above the photospheric inversion line. However, this is not always the case, probably because of its complex structure. Anyway, emission of an NLS is concentrated in the vicinity of a neutral line.

3.1. Identification of an NLS

An NLS at 17 GHz in AR 10488 is identified from its position, *i.e.*: (*i*) just above or close to the inversion line of the radial (vertical) magnetic field, B_r; (*ii*) at a locus of the maximum magnitude of the tangential (horizontal) magnetic field, $|B_t|$. An NLS is bright and compact, unlike weaker, diffuse sources, extended along neutral lines that are often observed at 17 GHz and also match criterion (*i*). Figure 4 shows relative positions of microwave sources and magnetic components for three days, demonstrating points (*i*) and (*ii*). The B_r and B_t magnetograms were extrapolated from the photospheric line-of-sight magnetograms to a height of 2 Mm, which is rather arbitrary, roughly corresponding to the transition region. Top row shows negatives of 17 GHz Stokes I images overlaid with contours of B_r magnetograms. Bottom row shows $|B_t|$ maps (also negatives) overlaid with the same B_r contours. Three columns correspond to three days: 30 October (a,d), 31 October (b,e), and 1 November (c,f), all between 03 and 05 UT.

There are two radio sources in Figure 4a – c. The western one is a normal gyroresonance source associated with the leading sunspot P1. Its brightness temperature decreases in three days from 0.7 MK to 0.3 MK. The eastern source is co-spatial with sunspot N1 on 30 October. On the next day, it shifts to the neutral line between sunspots P2 and N1, and transforms into an NLS. It dominates during 1 November; its brightness temperature is ≈ 1 MK. Comparisons of the top and bottom panels in Figure 4 show the NLS resides at the locus of the maximum magnitude of the horizontal magnetic component.

NLS are usually not detectable at 34 GHz and only appear during prominent radio bursts. Probably, the magnetic field is insufficient to provide detectable gyromagnetic emissions at this frequency under relatively quiet conditions.

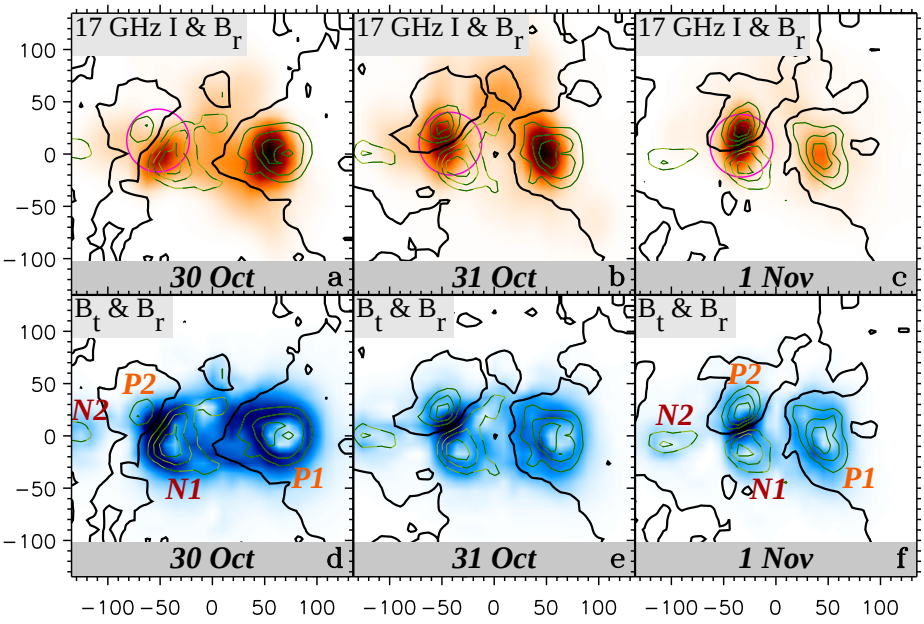

Figure 4. NLS at 17 GHz (a – c, background) and magnetic components at 2 Mm for three days (same in columns). B_r, green contours in all panels (solid positive, broken negative, thick black the neutral line); $|B_t|$, background in d – f. Contour levels are $\pm[300, 600, 900]$ G. All frames are centered at Carrington coordinates of $[-68°, 7.2°]$. Axes show arcseconds from the center. Magenta circles in panels a – c enclose the birthplace of the NLS, where the horizontal magnetic component $|B_t|$ reaches its maximum. Labels in panels d,f denote magnetic sources.

NLS are often well recognizable at 5.7 GHz. This is also the case for AR 10488. Figure 5 shows 5.7 GHz I maps as contours on top of B_r magnetograms from 29 October to 1 November, all between 03 and 05 UT. On 29 and 30 October, the brightest 5.7 GHz source (4.2 MK and 2 MK, respectively) is associated with the leading sunspot P1. On 31 October and 1 November, a new source (about 2 MK) dominates in the position close to the location of the 17 GHz NLS in Figure 4. Despite pronounced differences between 17 GHz and 5.7 GHz images, coincidence of the 5.7 GHz and 17 GHz sources both in space and time points at their association, *i.e.*, this component of the 5.7 GHz source is the NLS. Note, however, that a significant part of 5.7 GHz emission comes from larger areas corresponding to the fourth harmonic of the electron gyrofrequency. This component masks the NLS emission at 5.7 GHz.

3.2. Appearance of the NLS at 17 GHz and Microwave Fluctuations

As follows from Section 3.1, the NLS appears on 31 October. Figure 6 shows this process. Panels a – o present typical 17 GHz images of AR 10488 on 31 October, panels q – s show three of them for 1 November, and panels A, B show time profiles. P1, N1, and P2 in panels a, h, i, q label microwave sources over the corresponding sunspots. A pair of sources N1 and P2 constitutes a basis for the structure of the NLS. Interrelation of these sources and a loop-like structure

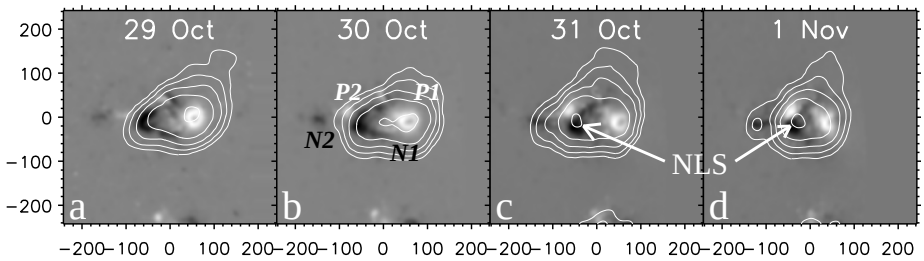

Figure 5. AR 10488: B_r magnetograms (background, bright N, dark S) overlaid by contours of Stokes I images at 5.7 GHz (SSRT). The brightness center of the 5.7 GHz source on 31 October and 1 November is approximately co-spatial with the 17 GHz NLS. Axes show arcseconds from the centers of frames corresponding to Carrington coordinates $[-67°, 8°]$.

connecting them shows up in small spiky radio bursts, which occur in this region. Their time profiles in panels A and B are labeled "NLS". The time profiles of the NLS and sunspot-associated source P1 were computed for areas presented in panels p for 31 October and t for 1 November. During the two first days of life, the NLS produces a lot of spiky fluctuations or small bursts. The time profile of the sunspot-associated source P1 is much steadier.

Images a – h (rows 1,2) show two spiky bursts (left shading in panel A). Frames a,b precede the first burst, frame c is close to its peak, and frame d shows its decay. Frame e is between the first and second spikes. Frames f – h show the rise, peak, and decay of the second spike. An additional source appears between N1 and P2 at the peak of the burst in frame c. Manifestations of a loop connecting N1 and P2 persist in frame d. The second burst occurs in footpoint P2.

Frames i – o (rows 3,4) show one more spike (right shading in panel A). Frames i, j show its onset and rise, frames k, l are close to its peak, and frames m – o show the decay. During the peak and decay, the loop-like structure is seen to connect sources N1 and P2. We call this structure hereafter the "NLS loop".

On 1 November, the 17 GHz NLS is an extended source between footpoints P2 and N1 of the NLS loop, with its brightness center being shifted to footpoint N1. As on the previous day, a new brightness center appears at peaks of some bursts, probably, near the top of the NLS loop. However, the shape of the NLS on this day does not significantly change during bursts and between them. As an example, frames q – s in the bottom row present a burst marked in panel B. The maximum brightness temperatures over frames are ≈ 1 MK before the burst, ≈ 2 MK near its peak, and ≈ 1.3 MK during the post-burst shoulder.

Time profiles of the NLS and sunspot-associated source P1 at 17 GHz are shown in Figure 6A for 31 October and Figure 6B for 1 November. Figure 6A represents a five-hour sequence of images produced with an interval of 60 seconds for 31 October. The microwave flux of the nascent NLS mainly increases, while the brightness temperatures of its components vary from 0.1 MK to 0.25 MK for source P2, from 0.5 MK to 0.35 MK for source N1, and from 0.07 MK to 0.35 MK for the middle part of the NLS (presumably the top of the NLS loop). As noted, the birth of the NLS was accompanied by large spiky fluctuations. The average interval between the spikes is about seven minutes, their typical

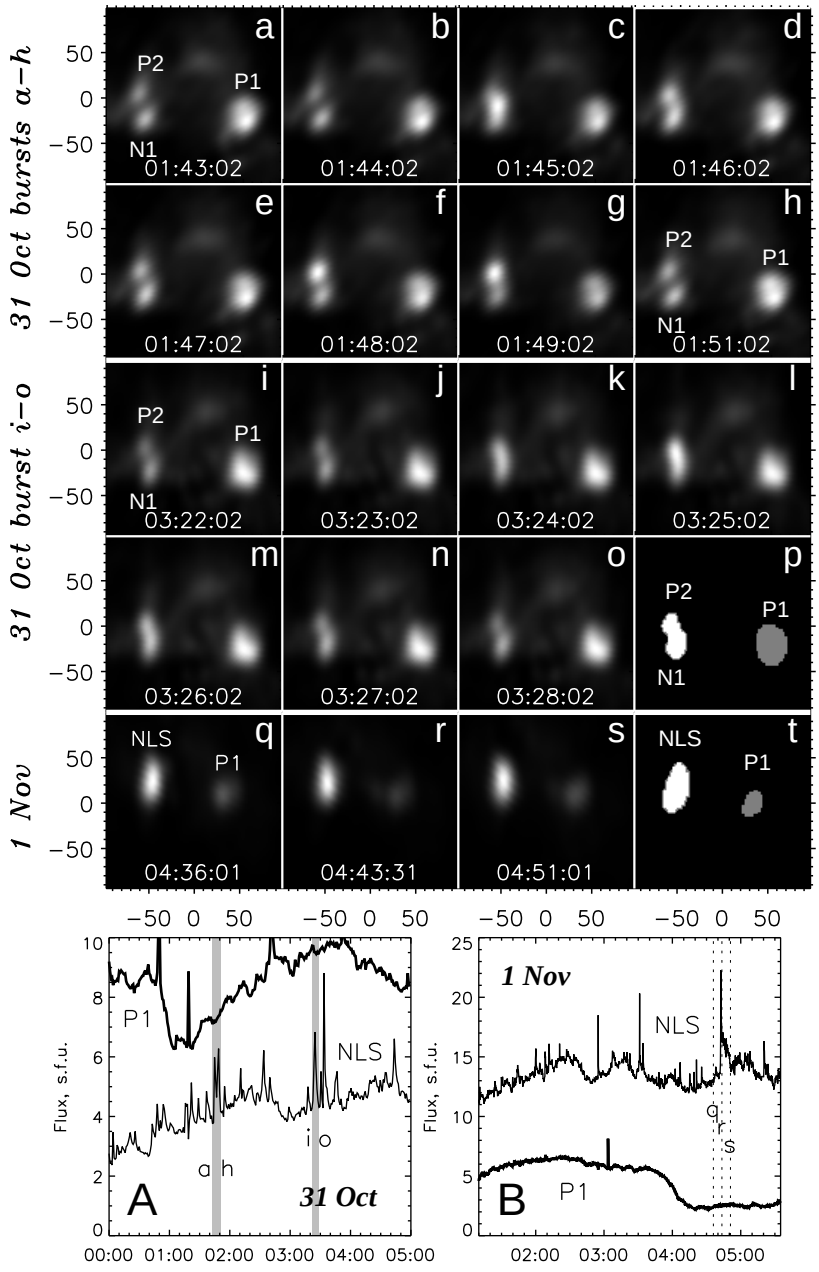

Figure 6. 17 GHz Stokes I images of small spiky bursts in the NLS (panels a – s) and their time profiles (panels A, B). Images show sources N1 and P2, which are the basis of the NLS, a loop between them, and the appearance of a loop top source. Spiky bursts on 31 October at 01:45 (a – h) and 03:25 (i – o); regions, over which total fluxes of the NLS and a sunspot-associated source are computed (p). Spiky burst on 1 November at 04:40 (q – s) and masks (t). A: time profiles for the NLS and sunspot-associated source P1 for 31 October. Shading marks intervals, for which images are shown. B: same for 1 November. Imaging intervals are 60 seconds for 31 October and 10 seconds for 1 November. Axes around images show arcseconds from centers of frames ($[508'', 81'']$ for 31 October and $[695'', 79'']$ for 1 November.)

duration is one – three minutes, and peak brightness temperatures do not exceed 1 MK.

Figure 6B represents a four-hour-long ten-second cadence sequence of images on 1 November. On that day, the gyroresonance source P1 produces a single burst, but does not exhibit quasi-periodical oscillations. At the same time, the NLS surpasses source P1 in total flux. The brightness temperature of the NLS exceeds 1 MK even without bursts, and it increases in bursts by 0.1 – 1.3 MK. The NLS maintains its burst activity; however, some changes occur with respect to the previous day. The relative magnitude of bursts decreases. Their typical duration also decreases by a factor of about six, *i.e.*, to 10 – 30 seconds. Their time profiles are smooth; an analysis of images produced with an interval of one second does not reveal any fine time structures.

3.3. Summary of Sections 3.1 and 3.2

The NLS appears at 17 GHz as a pair of radio sources N1 and P2. They are associated with converging sunspots of opposite polarity N1 and P2 initially belonging to different bipolar structures (Section 2). The NLS in the first days of its life produces a lot of weak bursts. The presence in microwave images of a loop-like structure connecting sources N1 and P2 and the appearance of a source between them lead to a conclusion that the emitting volume of a quasi-stationary 17 GHz NLS is of magnetic loop-like structure rooted in sunspots with strong magnetic fields. All these facts suggest that the NLS resides in the vicinity of a neutral line, where the horizontal magnetic component has a maximum. In principle, the observed brightness distribution along the NLS loop perhaps could be explained by distributions of the magnetic field strength, parameters of thermal plasmas and, probably, non-thermal electrons within the loop. However, there are more important questions. It is unclear why the emission of this complex, long-lived source is concentrated in a loop-like structure, and how this structure differs from other magnetic loops also rooted within a zone of strong magnetic fields of sunspots N1 and P2. If, for example, gyroresonance emission on the third and fourth harmonics of gyrofrequency is important in sources N1 and P2, then the plasma pressure in the NLS loop is higher than the surrounding one. At the same time, the appearance of a burst source in the middle part of the NLS loop as well as persistence of the emission of this part of the NLS loop indicate its similarity with an immovable flare loop. Figure 12a schematically shows location of such a loop rooted in footpoints N1 and P2 and observed during a weak spiky burst on 2 November at the same place, where an X2.7 flare starts on 3 November. The height of the loop top is ≈ 12 Mm, and its footpoint separation is ≈ 19 Mm.

4. X2.7 flare

The X2.7 flare (N08 W73) occurred in AR 10488 on 3 November, on the fourth day of the life of the NLS. The NLS brightens at about 00:58:30 and then transforms into a flare loop visible at both 17 and 34 GHz. The burst has three

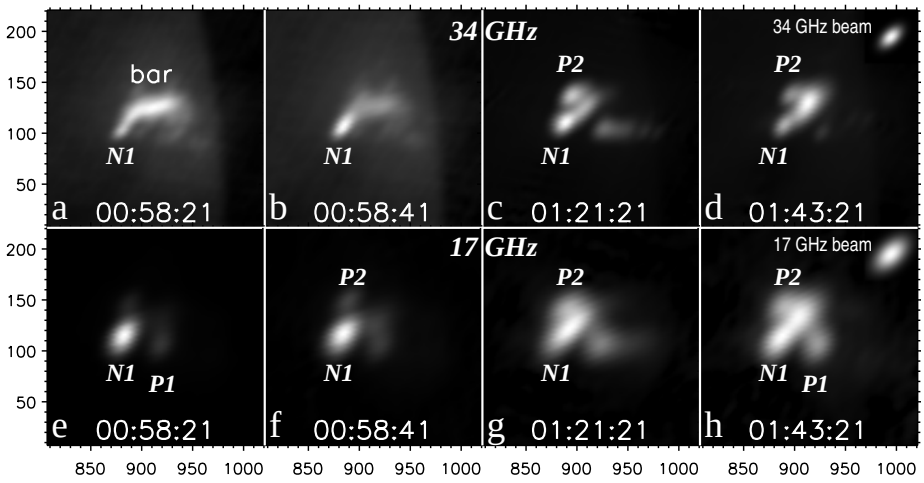

Figure 7. Stokes I images of AR 10488 before and during X2.7 flare at 34 GHz (upper row) and 17 GHz (lower row). The NoRH beam at the corresponding frequencies is shown in the upper right corners of frames d and h. Axes show arcseconds from the solar disk center.

main peaks at about 01:15:20, 01:21:00, and 01:32:40 (see the microwave time profile in Figure 9e). Its total duration is about three hours. The microwave flux reaches 700 sfu at 17 GHz and 950 sfu at 34 GHz. The maximum brightness temperatures reach 44 MK at 17 GHz and 15 MK at 34 GHz.

Figure 7 shows Stokes I images at 34 GHz (a – d) and 17 GHz (e – h) before (a, e) and during the flare. The brightness center of the NLS pre-flare emission at 17 GHz is displaced toward footpoint N1. At 34 GHz, the southern part of this loop and its footpoint N1 are visible together with an extended bar-like structure (labeled in frame a) pointed toward the west limb (see also Figure 10a). The brightness temperature of the NLS 20 seconds later increases from 2 MK to 6 MK at 17 GHz without pronounced changes of its spatial structure (frame f). At 34 GHz (frame b), a compact source appears in footpoint N1 with an increase of the brightness temperature from 0.04 MK to 0.25 MK. Frames c,g show a flare loop at about the second peak of the burst. Footpoints N1 and P2 significantly contribute to the 34 GHz emission. The brightness temperature in footpoint N1 reaches 12 MK. Just at that time RHESSI recorded strongest hard X-ray (HXR) emissions in bands of 100 – 300 keV and 300 – 800 keV. Note that at 34 GHz, the top of the flare loop dominates during the first peak, whereas its legs dominate during the third peak. During the decay phase (frames d and h), the source in the top of the rising loop dominates at both frequencies, while its footpoints almost coincide with those of the NLS loop, N1 and P2. Later on, the flare loop fades and then ceases as a post-flare arcade appears.

4.1. 34 GHz/Soft X-Ray Bar and a Current Sheet

The extended 34 GHz bar-like feature labeled in Figure 7a apparently stretches out of the NLS loop top. The southern part of this loop with its footpoint N1 is well visible (see also Figure 10). Figure 8 presents GOES/SXI soft X-ray images

of AR 10488 before the X2.7 flare (upper row), at its onset (frame e), and during its course (f – h). The bar in Figure 8e coinciding with the 34 GHz feature is bright in a GOES/SXI image; hence, it emits soft X-rays, and therefore it is hot. Its radial orientation suggests that it is a vertical structure rather than a horizontal one. One might ask if the bar might be associated with a horizontal structure, whose plane-of-sky projection were also directed radially, in particular, an arcade of small loops along a magnetic neutral line. However, as Figure 10a shows, the neutral lines of the radial magnetic field calculated either for the photospheric level, $h = 0$, or for a height of $h = 10$ Mm, have nothing to do with the bar. Also, EIT 195 Å images do not show anything similar to such an arcade, neither before the flare nor at its onset. The fact that the top of a rising flare loop moves throughout the flare exactly along the axis of the pre-flare bar also supports its vertical orientation, because tops of flare loops are known to usually apparently rise up. This flare is a typical LDE, which are known to be well described by a "standard flare model", in which tops of flare loops apparently rise along a current sheet. Thus, the bar might be related to a current sheet.

One might also ask why this bar is narrow, without lateral extensions, which would be expected for a current sheet. The reason is as follows: we are probably dealing with an arcade structure stretched out. In a 2- or 2.5-dimensional consideration, the configuration is supposed to continue beyond the plane discussed, which results in an infinitely extended slab-like current sheet above a photospheric neutral line (see also Figure 13b). In a real 3D situation, fixed-height lines of equal magnetic-field strengths are curved rather than straight. Centers of curvature correspond to projections of sunspots on their plane laying parallel to the photosphere. Surfaces connecting these lines are also curved. The distance between them (δx) is not constant. Vertical magnetic components on these surfaces are antiparallel; the thickness of a current sheet located in between also varies. The average current density, $j \propto i/\delta x$ (i the total electric current, independent of the cross section area), is maximal at a site, where the distance between the surfaces is minimal like a waist (*cf.* Birn *et al.*, 2000). The shape of this site should be close to a vertical, nearly straight bar. The rate of diffusion of magnetic fluxes at this site is maximal even with homogeneous plasma conductivity (σ), because the strongest Joule dissipation (j^2/σ) occurs here. Thus, the 34 GHz bar might well represent the volume of the strongest magnetic diffusion, or a diffusion region. It corresponds to volume within an extended pre-flare current sheet, where the rate of quasi-stationary magnetic reconnection is maximal.

The approaching sunspots N1 and P2, between which the NLS loop is located, are centers of curvature of the aforementioned surfaces. To the waist area between them there corresponds an almost vertical line originating from the junction of sunspots N1 and P2. We suggest that the 34 GHz bar is directed nearly along this line, that allows estimating the height of its upper end of $Z \approx 30 - 35$ Mm. Measurements of the observed bar provide its length of $L \approx 25$ Mm, a deconvolved cross-section width of $\Delta \approx 6$ Mm (supposed to be equal to its depth), and the brightness temperature of about 0.08 MK. The difference $Z - L \approx 10$ Mm apparently corresponds to the height of the NLS loop. Assuming the pre-flare emission of the bar at 34 GHz to be a thermal free-free

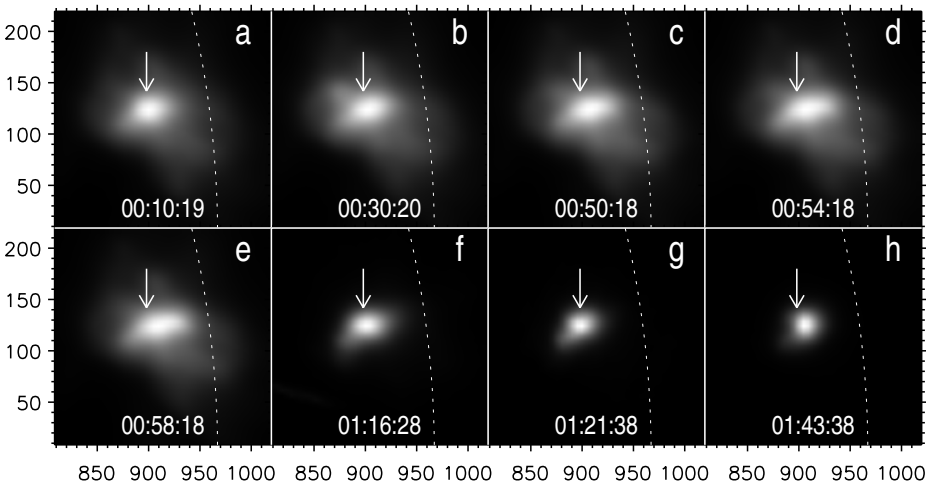

Figure 8. Soft X-ray GOES/SXI images observed before (a – e) and during (f – h) the X2.7 flare. An extended feature in frame e corresponds to the bar observed at 34 GHz (Figure 7a). The brightest feature in frames f – h corresponds to the source in the flare loop top. The position of the arrow in all frames is the same as in Figure 10a. Dotted lines denote the solar limb. Axes show arcseconds from the solar disk center.

one (optically thin), with a probable range of its kinetic temperatures of 3 – 9 MK, the plasma density is $(2-3)\times10^{10}$ cm^{-3}. An increased plasma density is believed to be a property of a quasi-stationary current sheet.

The bar visible at 34 GHz (Figure 7a) exists for $\gtrsim 0.5$ hours before the flare onset. Movies composed from one-second snapshots averaged over several (up to a few hundreds) frames show the bar to be a radially-extended variable structure, in which two features are slightly brighter than a diffuse background. The eastern feature lies in the bottom of the bar (the cross in Figure 10a). It is the initial position of the flare loop-top source observed at 34 GHz. Another, the western feature is located in the upper part of the bar. Imaging capabilities of the NoRH are insufficient to reveal a finer spatial structure of the bar (the beam FWHM at 34 GHz is $8'' \times 14''$ at 00:20 – 00:50, and the brightness temperatures of the discussed features are typically $\lesssim 0.08$ MK). Nevertheless, the bar is seen to slowly lengthen before the flare onset that also in GOES/SXI images in Figure 8a – e show. Note that the two brighter features on the bar are detectable in GOES/SXI one-minute images of the previous-day weak flare, with their positions corresponding to those of features visible at 34 GHz on 3 November.

The presence of the bar at 34 GHz and in soft X-rays before the flare and at its onset, obvious difference between the bar and the neutral line, and the rising motion of the top of the flare loop along this feature are consistent with the possibility that the bar represents a part of a vertical coronal current sheet.

4.1.1. Descending Polarization Feature and Ejection

Another interesting phenomenon, which probably reflects processes occurring in the current sheet, is illustrated in Figure 9. Panels (a – d) present 17 GHz Stokes

V images averaged to enhance their legibility. All polarized sources in AR 10488 are negatively (left-handedly) circularly polarized (LCP) before the flare (not shown here). This sense corresponds to the normal situation of the x-mode for a negatively polarized source southeast of the neutral line (shown as a green contour in Figure 9d), whereas it is opposite for negatively polarized sources westerly of the neutral line (closer to the limb). The latter fact is due to a well-known polarization reversal effect, which occurs in propagation of radio emission through a plasma region with a quasi-transversal magnetic field (QT-region).

At the onset of the burst, a compact, polarized radio source appears at the upper end of the bar. It is weaker than the major microwave sources. Complexity of the microwave structure during the burst makes it difficult to distinguish this source in total intensity. Fortunately, it is detectable at 17 GHz as a positively polarized feature visible in Figure 9a – d as a bright region. The cross in frames a – c corresponds to its brightness center in frame a. To emphasize this weak feature, we display the images using the 0.3 power for magnitudes of positive and negative pixels separately. The feature is real despite its weakness. The following facts support this. (*i*) Its brightness temperature in RCP well exceeds the noise and even the quiet Sun's level in total intensity, being always $> 20\,000$ K, and during the strongest burst emission it varies mostly between 60 000 K and 150 000 K, reaching 330 000 K. (*ii*) These values are between 1% and 18% of the brightest (LCP) source in a Stokes V frame, *i.e.*, within the dynamic range of the NoRH imaging routine (declared 25 dB or 0.3%). (*iii*) The feature persists in the same region for several hours, at least, up to 03:10. (*iv*) Its motion differs from the motion of sidelobes of the NoRH beam from brightest sources. Sometimes side lobes cross it, and sometimes not, as Figure 9c shows. It moves nearly along the pre-flare bar, but unlike the motion of the flare loop top by 01:15, having nothing to do with major sources at the same time and their motions. (*v*) The sense of its polarization corresponds to the direction of the magnetic field in this region (Figure 9d) without the reversal. (*vi*) The maximum and average degree of its polarization (over its area) is 20 – 25% and 8 – 10%, respectively, between 00:59 and 01:05, and then they vary within 5 – 10% (2 – 4%) until, at least, 02:30. All of these quantities are too high to be suspect. For all of these reasons, we conclude that this positively polarized feature is a real solar phenomenon rather than an instrumental effect or other artifact.

This feature appears between frames a and b of Figure 7. It moves from the western end of the pre-flare bar to its eastern end, toward the top of the flare loop, which already appears. Figure 9d presents its motion (black line) along with its maximum brightness temperature in RCP (red) and the total flux time profile at 17 GHz (gray thick). We measured its position along the E – W direction, which is close to the orientation of the bar. The perpendicular component of its motion is affected by a close, negatively polarized, strong source above the leading sunspot to the SouthSouthwest, that partly suppresses adjoining parts of the RCP feature. This causes a seeming bend of its trajectory to round the strong source from the north that does not appear to be real. Although we carefully co-aligned images, weakness of the feature and limited imaging capabilities of the NoRH restrict accuracy of measurements. In particular, gradual ascending

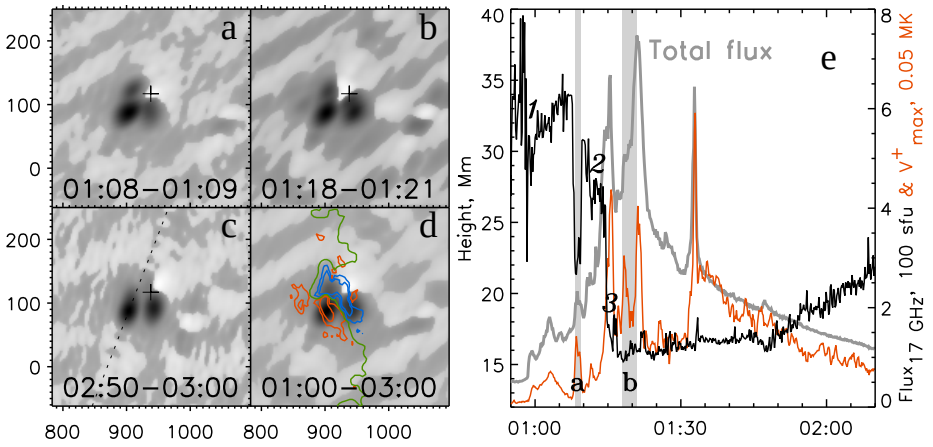

Figure 9. A weak polarization feature. Left (a – d): Stokes V images at 17 GHz averaged over various intervals during the X2.7 flare (all images are nonlinearly displayed, RCP is bright). Intervals for images a and b are shown with shading in panel e. The reference cross in frames a – c corresponds to the center of the positively polarized feature in frame a. A slanted dotted line in frame c traces sidelobes of the NoRH beam. Frame d is overlaid by contours of the photospheric magnetogram (blue N, red S, green the neutral line). Axes show arcseconds from the solar disk center. Right (e): the motion of the polarization feature (black), its maximum brightness temperature (Stokes V, red), and the total flux time profile at 17 GHz (thick gray). Labels 1 – 3 denote instants, for which the polarization feature is shown in Figure 10a. A jump from position 2 down to 3 occurs during the impulsive increase of the microwave flux.

trends during 01:00 – 01:07 and 01:18 – 01:45 are questionable, whereas jumps at 01:07 – 01:10 and 01:13 – 01:15 as well as the rise after 01:50 are certainly real.

As large scatter of the measurements by 00:58:30 indicates, this feature is not well detectable before the burst. The scatter decreases, when the feature becomes well pronounced at a height of 31 – 33 Mm estimated assuming its position to be on the vertical bar. The RCP feature moves by the first main peak (01:15) jumpingly. During a secondary peak at 01:08 – 01:09, it drops to a height of 22 – 23 Mm, and then gets up to a new position at 27 – 31 Mm (it is difficult to understand if the two positions within 01:10 – 01:15 are really distinct, or their difference is due to measurement problems). During the rise of the first main peak, this source falls to its minimum height of about 16 Mm to saddle up the top of the flare loop. Then they rise together for 2.5 hours.

The line-of-site magnetic component in the flare loop top visible at 17 and 34 GHz in total intensity is directed to the observer. The same direction has the line-of-site component on the photosphere behind this source. Correspondence of the positive polarization of the discussed feature to its native x-mode emission suggests that due to the its high location, its emission does not cross a QT-region, in which the polarization of emissions from adjacent sources reverses.

The emission mechanism of this feature is likely gyrosynchrotron from non-thermal electrons, because the degree of its polarization (up to 25% even with probable suppression from close, oppositely polarized major sources) as well as its maximum brightness temperature (a few MK in total intensity) are too high for thermal free-free emission (optically thin). Its time profile (red) is too

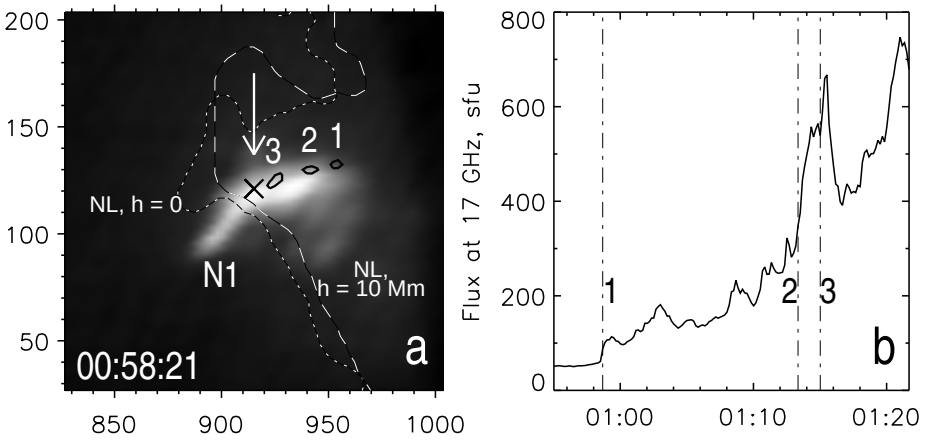

Figure 10. Left: 34 GHz image of the bar (background) overlaid by black contours of the polarization feature observed at different instants 1 – 3 marked in panel b. Broken lines show the neutral line (NL) at the photosphere and at 10 Mm (calculated). The cross marks a probable position of the NLS loop top, at which also the arrow points. Axes show arcseconds from the solar disk center. Right: a part of the total flux time profile of the flare at 17 GHz. Vertical lines mark instants, for which the contours of the polarization feature are shown in panel a.

impulsive, as Figure 9e shows. The emission seems to be mostly thermal after 01:45.

Figure 10a shows the bar at 34 GHz as grayscale background overlaid by black oval contours of the polarized feature observed at 00:58:41, 01:13:21, and 01:15:01. These instants are marked with dash-dotted vertical lines in Figure 10b and labeled in Figure 9e. As mentioned, after a drop to the lowest position (labeled 2 – 3) during the sharp rise of the microwave flux, this feature moves towards the top of the flare loop, whose center at this time is denoted with the cross in Figure 10. As one-minute GOES/SXI images show, in the same interval, the outer (western) part of the soft X-ray bar (Figure 8e – f) disappears and probably evolves into an ejection moving away along the axis of the bar. Figure 11a – d clearly shows its appearance (the arrow in frame b) and expansion (frames c and d). Note that the linear fit of a corresponding CME with a central position angle of 304° listed in the SOHO LASCO CME Catalog (http://cdaw.gsfc.nasa.gov/CME_list/) provides an extrapolated onset time of about 01:10 at $1R_{\odot}$. The remaining part of the bar becomes the top of the flare loop pointed by the arrow in Figure 8f. Arrows in all frames of Figure 8 have identical positions corresponding to the arrow in Figure 10a.

Our data set does not reveal a physical reason for association of the ejection with the downward motion of the polarized feature at the flare onset. This feature might represent a non-thermal source at the tops of magnetic loops traversing the diffusion region of a current sheet. Its jumps might reflect displacements of the site of the maximum reconnection rate along this region. Independent of correctness of these assumptions, it is important that these phenomena occur inside the bar-like structure just before the first main peak of the burst at 17 and 34 GHz. The most probable cause of the ejections is magnetic reconnection, in

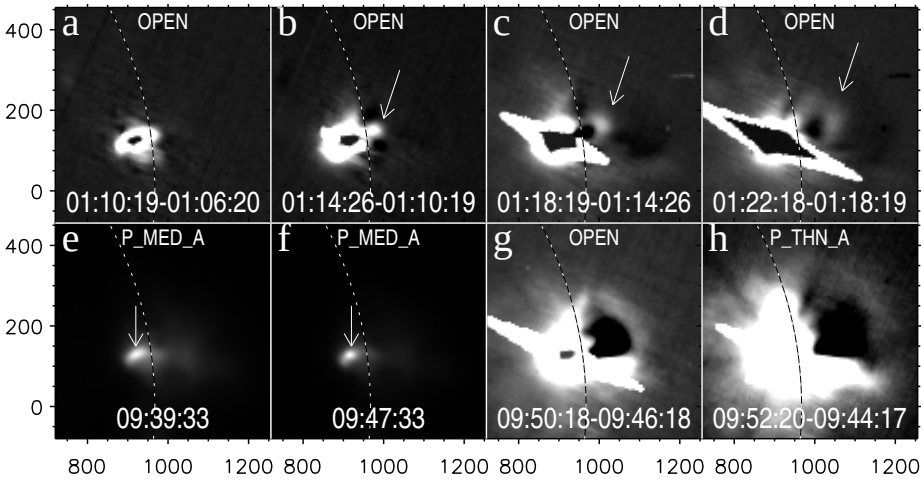

Figure 11. Analogy of the X2.7 and X3.9 events on 3 November in GOES/SXI images. Top (a – d): The appearance (b) and expansion (c, d) of a coronal ejection (pointed to by the arrow) in difference images of the X2.7 event. Bottom: the X3.9 event. (e, f): Non-subtracted images of AR 488 before (e) and at the onset (f) of the flare. The arrow indicates the initial position of a flare loop (*cf.* these frames with Figure 8e,f related to the X2.7 event). (g, h): Difference images reveal a coronal ejection. Frame g is similar to Figure 1a from Vršnak *et al.* (2006).

particular, tearing of the current sheet. Just after ejection of a magnetic island from a current sheet, both its acceleration and the rate of flare energy release reach their maxima, as theory predicts (see, *e.g.*, a generalized "standard flare model", Shibata, 1999) and observations confirm (Zhang *et al.*, 2001). These circumstances are consistent with our findings and the possibility that the bar-like structure represents a part of a current sheet.

4.1.2. Similarity with the X3.9 Flare

Another major event, an X3.9 flare, starts at the same place on the same day at 09:43. It is homologous with the preceding X2.7 flare. GOES/SXI images observed before the X3.9 flare and at its onset show an extended feature similar to the bar in Figure 8e, but it is shorter here. The arrow in Figure 11 points at its brighter eastern part before the flare (e) and at its onset (f). Its outer part disappears to transform into an ejection whose expansion is shown in frames g and h. It corresponds to a CME with a position angle of 293°, which is close to the preceding CME. The remaining eastern part of this feature becomes a loop-top source observed in soft X-rays during the rising phase of the flare similar to that preceding X2.7 event.

Veronig *et al.* (2006) addressed the X3.9 flare and also found a loop-top source in HXR RHESSI images of a few bands from 15 keV to 30 keV to descend during the rise phase of the HXR burst. Its height – time plot in their Figure 6b and black line in our Figure 9e after the time labeled 2 exhibit overall similarity. RHESSI 15 – 20 keV images in their Figure 9b also show ascension and subsequent disconnection of the outer part of the bar. There is a great deal of similarity between various aspects of these two homologous events, in particular, similar

behavior of the polarized feature in the X2.7 flare and the HXR loop-top source in the X3.9 flare. Veronig *et al.* (2006) also conclude that the picture of the X3.9 event is coherent with the "standard flare model" containing a vertical current sheet.

They explain the fall of the loop-top source by shrinkage of magnetic loops. It is expected to be gradual and monotonic, as their Fig. 6b shows. However, our Figure 9e shows that at earlier stages of the flare, well before the impulsive rise of its emission, the motion of the polarization feature is more complex. Its non-monotonic character is unlikely to be due to shrinkage of magnetic loops.

4.2. Summary of Section 4

Section 4 leads to a conclusion that the pre-flare bar-like feature, whose base coincides with the top of the NLS loop, is a part of a nearly vertical current sheet. This is supported by the following facts. No horizontal structures exist to mimic a radially extended bar. The bar is a hot, dense coronal structure. It lengthens up before the flare. The flare loop top rises along the axis of the bar. A polarized non-thermal microwave source descends along the bar, being apparently related with the coronal ejection.

In conclusion, Figure 12b schematically presents the position of the pre-flare bar under the main magnetic separator of AR 10488 (see Figure 3). On 3 November, the height of the potential-approach separator was ≈ 70 Mm.

5. Conclusion

The main structural component of a quasi-stationary NLS in AR 10488 is a magnetic loop-like structure, an NLS loop, whose footpoints are located in strong magnetic fields of converging sunspots. Its top is located at the bottom of a diffusion region, a part of a vertical coronal current sheet in which the rate of quasi-stationary magnetic reconnection is maximal. Persistent input of heat, plasma and, probably, non-thermal particles in the NLS loop is the cause of its enhanced microwave emission. An extended current sheet, strong magnetic field, and suitable conditions in the photosphere favor occurrence of a powerful flare. All of these items shed light on the nature of an NLS and physical background of an empirical connection between the appearance of a bright NLS and occurrence of a major flare in one – three days. Figures 12 and 13 illustrate our major results.

Figures 12a,b show our findings from observations: the NLS loop under the main magnetic separator (a) and the bar-like feature (b), a microwave indicator of a diffusion region inside a pre-flare current sheet. Comparison of images (a) and (b) reveals the top of the NLS loop at the bottom of a current sheet.

Figure 13 presents theoretical expectations. Figure 13a shows the NLS loop below the X-point to ease understanding Figure 13b. In the potential-field approach, a current sheet is absent, plasma parameters in the NLS loop do not differ from its environment, and a microwave NLS does not exist. Figure 13b sketches out a pre-flare current sheet (a rectangle extended upward) and the NLS loop at its base. Here, the background image reproduces Figure 7 from

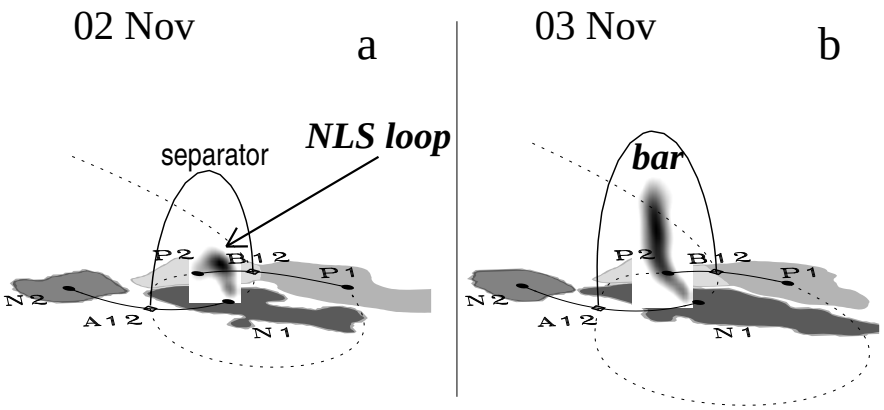

Figure 12. A collage of AR 10488. (a) The NLS loop under the main magnetic separator of the potential-field approach (thick) on 2 November. (b) The bar at 34 GHz under the separator on the next day. The bar is a vertical part of a current sheet before the X2.7 flare. Comparison of (a) and (b) reveals the top of the NLS loop at the bottom of the bar.

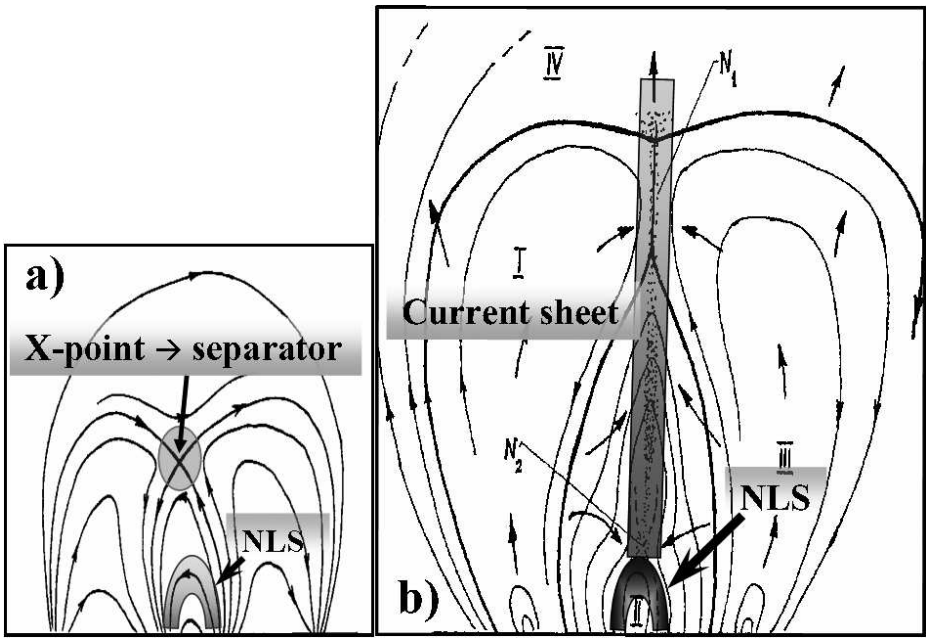

Figure 13. A cartoon of magnetic configurations. (a) A quadrupolar configuration in two dimensions. The position of the NLS loop under an X-point is shown schematically. In three dimensions, the X-point is replaced by a magnetic separator shown in Figure 12. If a current sheet is absent, then plasma parameters in the NLS loop do not differ from the environment, and there is no NLS. (b) Expansion of the magnetosphere of the active region and formation of an extended current sheet (vertical bar). The density of electric current integrated over thickness of the current sheet is maximal not in a vicinity of a potential-approach X-point, but in the lower part of the current sheet. The top of a quasi-stationary NLS loop-like structure is located in its bottom.

Uralov (1996b) showing one of stages in evolution of expanding magnetosphere of an active region, *i.e.*, a descending current sheet with one magnetic island.

The physical aspect of the NLS problem presented in Figure 13 was shown in Figures 15 and 16 from Uralov *et al.* (2000). In that paper, a vertical bar structure was found in soft X-ray *Yohkoh*/SXT images (Figure 10 of that paper) to evolve from an NLS a few hours before an X9 flare on 2 November 1992. It was strikingly similar to the bar found in the present study. That bar was denser and hotter than its environment and was interpreted as a part of a vertical non-neutral current sheet. However, in that study it was not possible to reveal the structure and behavior of the NLS; to follow the appearance of microwave flare emissions in the NLS and to distinctly observe the flare loop at 17 and 34 GHz, including its footpoints; and to use high-quality magnetograms and analytical methods of their analysis. The present paper has addressed these issues.

Acknowledgements We thank the teams of the Nobeyama Radioheliograph, the Siberian Solar Radio Telescope, the GOES Soft X-ray Imager, and the Michelson Doppler Imager on SOHO. SOHO is a project of international cooperation between ESA and NASA. We are grateful to S.M. White and L.K. Kashapova for useful discussions and assistance. A.U. and V.G. thank K. Shibasaki and his colleagues for invitation to Nobeyama Radio Observatory and hospitality during theirs visit to Nobeyama, where the main part of this study was done. We thank the anonymous reviewer for useful remarks. The study is supported by the Russian Foundation of Basic Research (06-02-16239, 06-02-16295, and 07-02-00101), and the programs of the Russian Academy of Sciences "Solar Activity and Physical Processes in the Sun-Earth System" and "Plasma Heliophysics".

References

Akhmedov, S.B., Borovik, V.N., Gelfreikh, G.B., Bogod, V.M., Korzhavin, A.N., Petrov, Z.E., Dikij, V.N., Lang, K.R., Willson, R.F.: 1986, *Astrophys. J.* **301**, 460.

Alissandrakis, C.E., Gel'frejkh, G.B., Borovik, V.N., Korzhavin, A.N., Bogod, V.M., Nindos, A., Kundu, M.R.: 1993, *Astron. Astrophys.* **270**, 509.

Birn, J., Gosling, J.T., Hesse, M., Forbes, T.G., Priest, E.R.: 2000, *Astrophys. J.* **541**, 1078.

Borovik, V.N., Vatrushin, S.M., Korzhavin, A.N.: 1989, *Bull. Special Astrof. Obs. North Caucasus* **28**, 118.

Chiuderi Drago, F., Alissandrakis, C.E., Hagyard, M.: 1987, *Solar Phys.* **112**, 89.

Démoulin, P., Henoux, J.C., Priest, E.R., Mandrini, C.H.: 1996, *Astron. Astrophys.* **308**, 643.

Gelfreikh, G.B.: 1985, In: Fomichev, V.V. (ed.), *The Physics of the Solar Flares*, Nauka, Moscow, 111.

Grechnev, V.V., Lesovoi, S.V., Smolkov, G.Ya., Krissinel, B.B., Zandanov, V.G., Altyntsev, A.T., Kardapolova, N.N., Sergeev, R.Y., Uralov, A.M., Maksimov, V.P., Lubyshev, B.I.: 2003, *Solar Phys.*, **216**, 239.

Hill, S.M., Pizzo, V.J., Balch, C.C., Biesecker, D.A., Bornmann, P., Hildner, E., Lewis, L.D., Grubb, R.N., Husler, M.P., Prendergast, K. *et al.*: 2005, *Solar Phys.* **226**, 255.

Korzhavin, A.N., Vatrushin, S.M.: 1989, In: Somov, B.V., Fomichev, V.V. (eds.), *The Physics of the Solar Plasma*, Nauka, Moscow, 100.

Kundu, M.R., Alissandrakis, C.E.: 1984, *Solar Phys.* **94**, 249.

Kundu, M.R., Velusamy, T. 1980, *Astrophys. J.* **240**, 63L.

Kundu, M.R., Alissandrakis, C.E., Bregman, J.D., Hin, A.C.: 1977, *Astrophys. J.* **213**, 278.

Kundu, M.R., Schmahl, E.J., Rao, A.P.: 1981: *Astron. Astrophys.* **94**, 72.

Lee, J., White, S.M., Gopalswamy, N., Kundu M.R.: 1997, *Solar Phys.* **174**, 175.

Longcope, D.W., Silva, A.V.R.: 1998, *Solar Phys.* **179**, 349.

Low, B.C., Lou, Y.Q.: 1990, *Astrophys. J.* **352**, 343.
Nakajima, H., Nishio, M., Enome, S., Shibasaki, K., Takano, T., Hanaoka, Y., Torii, C., Sekiguchi, H., Bushimata, T., Kawashima, S., Shinohara, N., Irimajiri, Y., Koshiishi, H., Kosugi, T., Shiomi, Y., Sawa, M., Kai, K.: 1994, *Proc. IEEE*, **82**, 705.
Rudenko, G.V.: 2001, *Solar Phys.* **198**, 5.
Rudenko, I.G., Rudenko, G.V., Uralov, A.M.: 2007, In: Bogod, V.M., Golubchina, O.A., Kaltman, T.I., Tokhchukova, S.Kh. (eds.), *Proc. All-Russian Conf. on Multi-Wavelength Investigations of the Sun and Modern Problems of the Solar Activity*, Spec. Astrophys. Obs., St. Petersburg, Russia, 462.
Sakurai, T.: 1982, *Solar Phys.* **76**, 301.
Scherrer, P.H., Bogart, R.S., Bush, R.I., Hoeksema, J.T., Kosovichev, A.G., Schou, J., Rosenberg, W., Springer, L., Tarbell, T.D., Title, A. *et al.*: 1995, *Solar Phys.* **162**, 129.
Schrijver, C.J., Derosa, M.L., Metcalf, T.R., Liu, Y., McTiernan, J., Régnier, S., Valori, G., Wheatland, M.S., Wiegelmann, T.: 2006, *Solar Phys.* **235**, 161.
Shibata, K.: 1999, In: Bastian, T.S., Gopalswamy, N., Shibasaki, K. (eds.), *Nobeyama Symposium on Solar Physics with Radio Observations*, NRO Report No. 479, 381.
Smolkov, G.Y., Pistolkors, A.A., Treskov, T.A., Krissinel, B.B., Putilov, V.A.: 1986, *Astrophys. Spa. Sci.* **119**, 1.
Strong, K.T., Alissandrakis, C.E., Kundu, M.R.: 1984, *Astrophys. J.* **277**, 865.
Sych, R.A., Uralov, A.M., Korzhavin, A.N.: 1993, *Solar Phys.* **144**, 59.
Uralov, A.M., Sych, R.A., Lubyshev, B.I., Nefedyev,V.P., Golovko, A.A., Korobova, Z.B., Alissandrakis, C.E., Smartt, R.N., Zhang Hongqi: 1996a, *Issledovaniya po geomagnetizmu, aeronomii i fizike Solntsa*, Nauka, Novosibirsk, **104**, 23.
Uralov, A.M.: 1996b, *Solar Phys.* **168**, 311.
Uralov, A.M., Sych, R.A., Shchepkina, V.L., Zubkova, G.N., Smolkov, G.Ya.: 1998, *Solar Phys.* **183**, 359.
Uralov, A.M., Nakajima, H., Zandanov, V.G., Grechnev, V.V.: 2000, *Solar Phys.* **197**, 275.
Uralov, A.M., Rudenko, G.V., Rudenko, I.G.: 2006a, *Publ. Astron. Soc. Japan.* **58**, 21.
Uralov, A.M., Rudenko, G.V., Rudenko, I.G.: 2006b, *Izvestiya Rossiiskoi akademii nauk, Fizika (Russian Physical Bulletin)*, **70**, 1475.
Uralov, A.M., Rudenko, G.V., Grechnev, V.V., Rudenko, I.G., Nakajima, H., Shibasaki, K.: 2007, In: Bogod, V.M., Golubchina, O.A., Kaltman, T.I., Tokhchukova, S.Kh. (eds.), *Proc. All-Russian Conf. on Multi-Wavelength Investigations of the Sun and Modern Problems of the Solar Activity*, Spec. Astrophys. Obs., St. Petersburg, Russia, 484.
Veronig, A.M., Karlický, M., Vršnak, B. Temmer, M.; Magdalenic, J., Dennis, B.R., Otruba, W., Pötzi, W.: 2006, *Astron. Astrophys.* **446**, 675.
Vršnak, B., Warmuth, A., Temmer, M. Veronig, A., Magdalenic, J., Hillaris, A., Karlický, M.: 2006, *Astron. Astrophys.* **448**, 739.
Zhang, J., Dere, K.P., Howard, R.A., Kundu, M.R., White, S.M.: 2001, *Astrophys. J.* **559**, 452.